with mouse T cell receptor Vβs. Alternatively, TSST may react with only one member of the $V_\beta 5$ family. Thus, in responses to TSST, the increase in blasts bearing this member may be offset by a disappearance of T cells bearing other members of the family, but also reactive with 1C1. Discrimination by superantigens among different members of Vβ families has been seen in mice, where the self superantigen Mls-1^a stimulates T cells positive for $V_\beta 8.1$ but not those bearing $V_\beta 8.2$ or $V_\beta 8.3$ (*12*), and SEC1 stimulates T cells bearing $V_\beta 8.2$ but not those bearing $V_\beta 8.1$ or $V_\beta 8.3$ (*13*).

In some experiments, the percentages of T cells that stained with anti-CD4 or anti-CD8 were checked before and after stimulation. The starting percentages were virtually unchanged by toxin stimulation. T cells from one donor, for example, were initially 78% $CD4^+$ and 23% $CD8^+$. After stimulation with the nine different toxins the percentages in the blasts of $CD4^+$ cells ranged from 74% to 79%, and of $CD8^+$ cells from 20% to 26%, suggesting that all these stimuli affected CD4 and CD8 cells equally. It might have been expected that the toxins, which are dependent on class II MHC for presentation (*3–6*), would have preferentially stimulated $CD4^+$ cells, but such is not the case. This result is in line with our findings in analogous systems in mice (*5*).

One of the most striking features of the data in Fig. 2 is the consistency of the results from one individual to another. Thus, although the five people tested had different HLA types and different starting percentages of T cells bearing the various Vβs (Table 1), the proportional changes in Vβ expression in blasts stimulated by each toxin were almost the same from one individual to another. These properties are similar to those we and others have described for superantigen stimulation of T cells in mice (*5, 6, 14*). Although the superantigens require class II MHC for presentation, the allele of class II has much less impact on superantigen presentation than it does on recognition of conventional antigens plus MHC by T cells.

These results show that the staphylococcal toxins are not indiscriminate mitogens for human T cells, but are, in fact, Vβ-specific, as they are for murine T cells (*5, 6*). This result accounts for the previously noted clonal specificity for such toxins (*4*). Although each toxin is able to stimulate only a subpopulation of all T cells in man, they are still powerful T cell stimulants, active at low concentrations. Some or all of the toxic effects of these proteins in man may be mediated by their ability to stimulate large numbers of human T cells. For example, the ability of these toxins to induce secretion of large quantities of lymphokines (*15*) is probably secondary to their ability to stimulate, in a Vβ-specific way, a sizable percentage of T cells. It is also possible that the ability of these and other microbial-derived superantigens to stimulate populations of T cells bearing particular Vβs may be related to the differential resistance of different individuals to the effects of these toxins and also to the ability of microbial attack to induce immune consequences, such as autoimmunity, in certain individuals.

REFERENCES AND NOTES

1. M. S. Bergdoll, in *Food-Borne Infections and Intoxications*, H. Riemann and F. L. Bryan, Eds. (Academic Press, New York, ed. 2, 1979), p. 443; L. Spero, A. Johnson-Winger, J. J. Schmidt, in *Handbook of Natural Toxins*, C. M. Hardegree and A. T. Tu, Eds. (Dekker, New York, 1988), p. 131; J. K. Todd, *Clin. Microbiol. Rev.* **1**, 432 (1988).
2. D. L. Peavy *et al.*, *J. Immunol.* **105**, 1453 (1970); M. P. Langford *et al.*, *Infect. Immun.* **22**, 62 (1978); T. Zehavi-Willner and G. Berke, *J. Immunol.* **137**, 2682 (1986).
3. R. Carlsson *et al.*, *J. Immunol.* **140**, 2484 (1988).
4. B. Fleischer and H. Schrezenmeier, *J. Exp. Med.* **167**, 1697 (1988).
5. J. White *et al.*, *Cell* **56**, 27 (1989).
6. C. A. Janeway, Jr., *et al.*, *Immunol. Rev.* **56**, 61 (1989).
7. B. L. Kotzin *et al.*, *J. Immunol.* **127**, 931 (1981).
8. H. Yssel *et al.*, *Eur. J. Immunol.* **16**, 1187 (1986); J. Borst *et al.*, *J. Immunol.* **139**, 1952 (1987).
9. D. N. Posnett, C. Y. Wang, S. M. Friedman, *Proc. Natl. Acad. Sci. U.S.A.* **83**, 7888 (1986); Y. Li, P. Szabo, M. A. Robinson, D. N. Posnett, abstract for the American Federation for Clinical Research (1989).
10. S. Carrel *et al.*, *Eur. J. Immunol.* **16**, 649 (1986).
11. R. Bigler, D. Fisher, C. Wang, E. Rinndoy Kan, H. Kunkel, *J. Exp. Med.* **158**, 1000 (1983). S511 was identified as an antibody to members of the human $V_\beta 12$ antibody as follows. RNA was prepared from T cell blasts after stimulation with S511 or anti-CD3 (legend to Fig. 1). Complementary DNA was prepared from this RNA and amplified by a quantitative polymerase chain reaction (PCR) with primers built to match analogous sense sequences for each of the known human Vβs and an antisense sequence in Cβ. A 3′ antisense and 5′ sense Cα oligonucleotide were used in each reaction to synthesize control Cα DNA. DNA so prepared was separated by electrophoresis in 2% agarose gels, blotted onto nitrocellulose filters, and probed with kinased oligonucleotides for Cα and Cβ. Material prepared from anti-CD3–stimulated blasts yielded a PCR product detectable with the Cβ probe after amplification with most of the Vβ oligomers. Material prepared from S511-stimulated blasts yielded a major Cβ probe–detectable product after amplification with a $V_\beta 12$ oligonucleotide and little detectable product after amplification with any other Vβ oligonucleotide. Details of this methodology will appear elsewhere (Y. Choi *et al.*, in preparation). RNA and cDNA preparation and quantiative PCRs were carried out as described in the following: J. M. Chirgwin, A. E. Przybyla, R. J. MacDonald, W. J. Rutter, *Biochemistry* **18**, 5294 (1979); U. Gubler and B. J. Hoffmann, *Gene* **25**, 263 (1983); R. K. Saiki *et al.*, *Science* **239**, 487 (1988); J. Chelly, J. C. Kaplan, P. Maire, S. Gautron, A. Kahn, *Nature* **333**, 858 (1988). Vβ-specific oligonucleotides were constructed to match sequences described by P. Concannon, L. A. Pickering, P. Kungand, and L. Hood [*Proc. Natl. Acad. Sci. U.S.A.* **83**, 6598 (1986)] and B. Toyonaga and T. W. Mak, *Annu. Rev. Immunol.* **5**, 585 (1987).
12. J. W. Kappler *et al.*, *Nature* **332**, 35 (1988).
13. J. Callahan, J. Kappler, P. Marrack, unpublished observations.
14. R. Abe and R. J. Hodes, *J. Immunol.* **140**, 4132 (1988); C. A. Janeway, Jr., *et al.*, *Immunol. Today* **9**, 125 (1988); C. A. Janeway, Jr., and M. Katz, *J. Immunol.* **134**, 2057 (1985); H. R. MacDonald *et al.*, *Nature* **332**, 40 (1988); D. Lynch *et al.*, *Eur. J. Immunol.* **16**, 747 (1986); A. M. Pullen *et al.*, *Nature* **335**, 796 (1988).
15. J. Kaplan, *Cell. Immunol.* **3**, 245 (1972); R. Carlsson and H. O. Sjogren, *ibid.* **96**, 175 (1985); T. Ikejima *et al.*, *J. Clin. Invest.* **73**, 1312 (1984); V. V. Micusan *et al.*, *Immunology* **58**, 203 (1986).
16. J. W. Kappler *et al.*, *Cell* **49**, 273 (1987).

17. Supported by PHS grants AI-18785, AI-17134, AI-22295, CA-42046, and AI/CA-26490 and by a grant from the W. W. Smith Charitable Trust. E.W.G. is a scholar of the Raymond and Beverly Sackler Foundation.

23 February 1989; accepted 20 April 1989

Transmembrane Channels Based on Tartaric Acid–Gramicidin A Hybrids

CHARLES J. STANKOVIC,* STEFAN H. HEINEMANN,†‡
JOSE M. DELFINO, FREDERICK J. SIGWORTH, STUART L. SCHREIBER*†

The gramicidin A transmembrane channel is believed to consist of two head-to-head β helices. Computer-generated models were used to formulate the structure of new single-chain channel molecules based on the gramicidin motif. The chemical synthesis of two tartaric acid–gramicidin A hybrids and single-channel analyses of their conducting properties are reported. These studies illustrate the rational design and synthesis of long-lived channels with tunable conductance properties and provide support for current molecular models of the natural (dimeric) gramicidin channel.

TRANSMEMBRANE CHANNELS SERVE as the conduits through which ions may traverse a cellular membrane. The naturally occurring peptide antibiotic gramicidin A [gA (*1*), OHCHN-L-Val-Gly-L-Ala-D-Leu-L-Ala-D-Val-L-Val-D-Val-L-Trp-D-Leu-L-Trp-D-Leu-L-Trp-D-Leu-L-Trp-$CONHCH_2CH_2OH$] conducts monovalent cations across lipid bilayers. Its study, which has stimulated a considerable body of research (*2*), has shown that gA dimers are the functional transmembrane elements (*3*). The solid-state structures of free (*4*) and cesium chloride–complexed (*5*) gA dimers

were recently reported. These are double-stranded antiparallel helical molecules that differ from one another in their helix dimensions. However, the active channel conformation is a head-to-head dimer of two $\beta^{6.3}$ helices (Fig. 1A). The evidence to support the head-to-head, single-stranded dimer (versus the double-stranded dimer) as the ion-transporting conformer is compelling (*3, 6*). For example, covalently N-linked dimers (malondiamide connector) form long-lived conducting channels (*7*). The antiparallel duplex structures found in the solid state cannot accommodate a malonyl linkage of the remote (about 30 Å) amino termini. Less certain, however, is the precise geometry of the channel structure. For example, a justable conductance properties (*10*).

In the model building studies, we used the coordinates of the right-handed (Ovchinnikov) and left-handed (Urry) β-helix gA dimers developed by Roux and Karplus (*11*) as the input structures. The left-handed β helix (*12*) is illustrative (Fig. 2A). A rigid (ring-constrained) dicarboxylic acid was sought with a geometry that was, after diamide cross-linking, complementary to the void formed upon removal of the amino-terminal formyl residues. These requirements were met by monocyclic 1,2-*trans*-dicarboxylic acids.

A symmetrically substituted monocycle is readily available from either enantiomer of diethyl tartrate (Scheme 1) (*13*). The (*S*,*S*)-

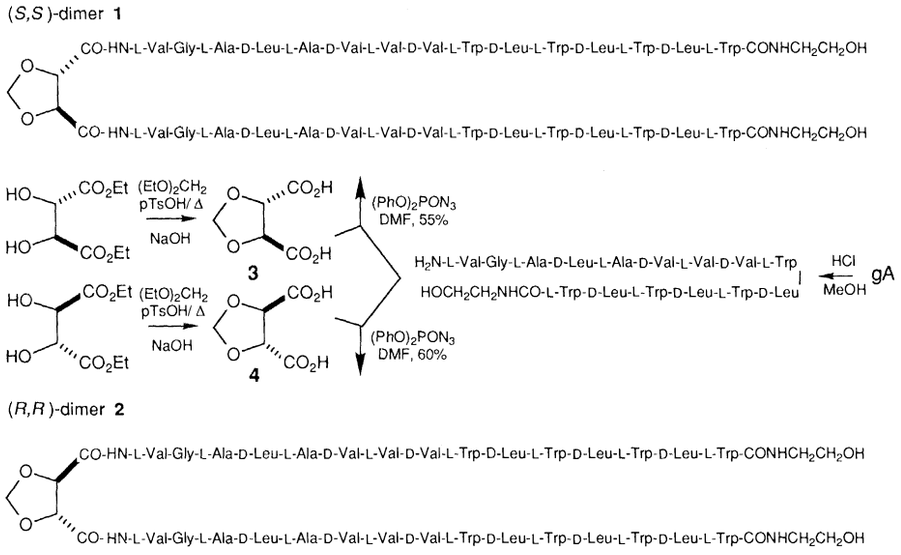

Scheme 1

debate exists concerning the handedness of the single helix (right versus left), and evidence has been presented in support of either possibility (*8, 9*).

In this study a probe of channel geometry involving the linkage of two desformyl gA units to nonracemic and C_2-symmetric dicarboxylic acids derived from (*S*,*S*)- and (*R*,*R*)-tartaric acids was designed and examined. The results of this exercise support current molecular models of the natural gA channel structure and illustrate the rational design of long-lived ion channels with ad-

1,3-dioxolane dicarboxylic acid (**3**) serves as the matched partner to gA [note that the (*S*,*S*)-stereochemistry of **3** corresponds to a truncated D,D-dipeptide and thus maintains the β-helix requirement for alternating amino acid stereochemistry; linkage occurs to the amino-terminal L-amino acid of gA],

Table 1. Rate constants for the permeation of K^+ through the investigated gA compounds. For natural gA the six free parameters of the two-site, three-barrier model [the association/dissociation rate of the first ion (f_1/r_1) and of the second ion (f_2/r_2), the rate of translocation over the central barrier (t_r), and the relative position of the binding site in the electrical field (Rel. el. dist.)] were fitted to a set of conductance data for KCl concentrations ranging from 20 to 1280 m*M* and membrane potentials ranging from 50 to 400 mV (not shown), in addition to the *I-V* curve (Fig. 5A) by least-squares methods. Starting with this set of parameters, we fitted the *I-V* curves of the (*S*,*S*)-linked gA (Fig. 5B) and the (*R*,*R*)-linked gA (Fig. 5C). The rms values indicate the deviation between theoretical functions and the observed *I-V* curves shown in Fig. 5. Although each fit is based on a single *I-V* curve, the main difference between the rates for (*S*,*S*)- and (*R*,*R*)-linked gA is a strong decrease in t_r.

Parameter	Natural gA	(*S*,*S*)-linked dimer	(*R*,*R*)-linked dimer
f_1	2.1×10^8	2.9×10^8	3.5×10^8
r_1	1.2×10^7	1.9×10^7	1.1×10^7
t_r	2.2×10^7	2.0×10^7	6.2×10^5
f_2	1.4×10^8	6.8×10^7	2.9×10^7
r_2	1.3×10^8	1.1×10^8	5.1×10^8
Rel. el. dist.	0.079	0.099	0.063
rms (pA)	0.046	0.038	0.039

whereas linkage of gA to the (*R*,*R*)-enantiomorph (**4**) was expected to produce a mismatched combination (Fig. 2, B, C, and D). In the latter case, diamide formation should result in a disruption of an idealized peptide backbone geometry at the critical head-to-head combining site (*14*). For the (*R*,*R*)-mismatched linker, two energetically favorable conformations were found. One places the dioxolane ring of the linker outside the helix, whereas the other places this element inside the helix (Fig. 2, C and D). In either case, a structure results with a disturbance at the center of the channel. For the (*R*,*R*)-conformer depicted in Figs. 2C and 3B, the root-mean-square (rms) deviation of nearest

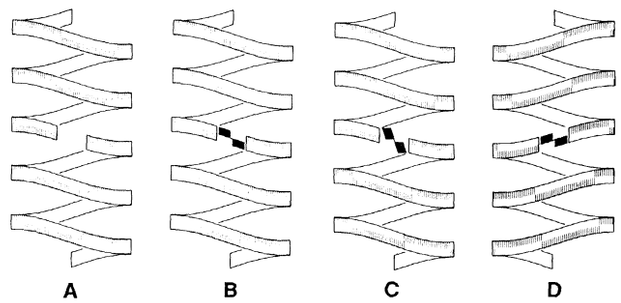

Fig. 1. Ribbon diagrams of the left-handed (A, B, and C) and right-handed (D) helices of gA dimers. The alternating stripes indicate the alternation of the orientation of the carbonyl vectors, and the linkers are fitted to maintain this alternating sequence, thereby maintaining the intermonomer hydrogen-bonding pattern that stabilizes the continuous helix through the bilayer. (**A**) Left-handed gA with no linker, representing natural gA. (**B**) Left-handed gA with the (*S*,*S*)-linker, representing the matched pair. (**C**) Left-handed gA with the (*R*,*R*)-linker, representing the mismatched pair. (**D**) Right-handed gA with the (*S*,*S*)-linker, again representing the matched pair.

C. J. Stankovic and S. L. Schreiber, Department of Chemistry, Yale University, New Haven, CT 06511.
S. H. Heinemann and F. J. Sigworth, Department of Physiology, Yale School of Medicine, New Haven, CT 06510.
J. M. Delfino, Department of Molecular Biophysics and Biochemistry, Yale University, New Haven, CT 06511.

*Present address: Department of Chemistry, Harvard University, Cambridge, MA 02138.
†To whom correspondence should be addressed.
‡Present address: Max-Planck-Institut für biophysikalische Chemie, Abteilung Membranbiophysik, D-3400 Göttingen, Federal Republic of Germany.

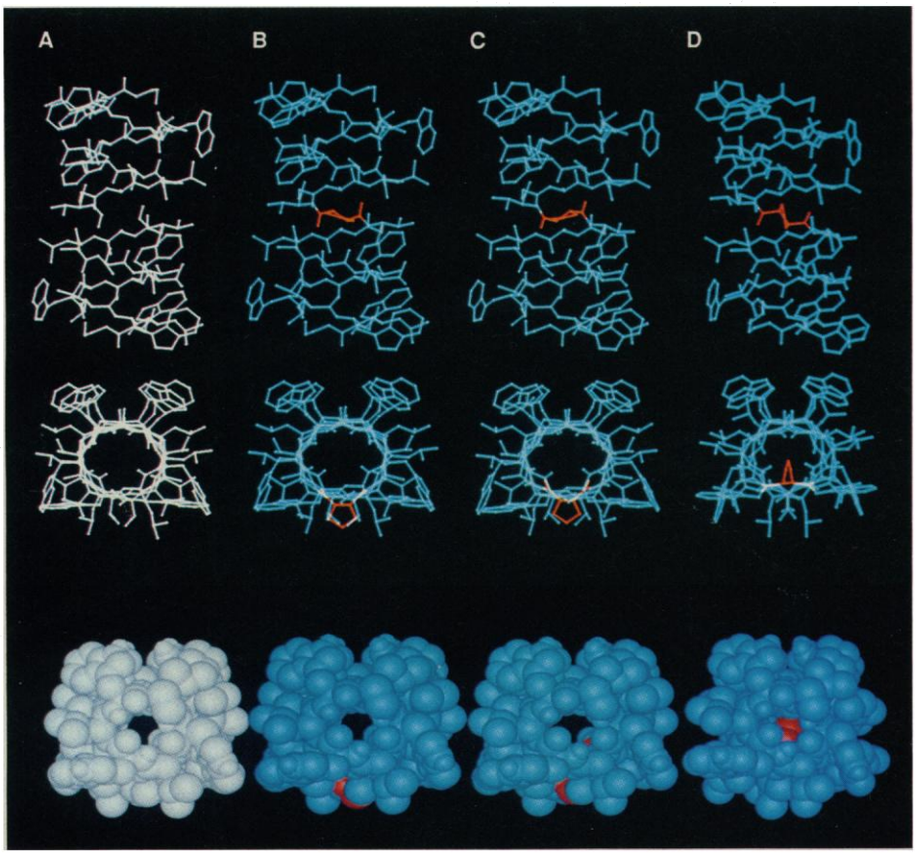

Fig. 2. Computer-generated models based on theoretical coordinates of natural gA and the linked dimers reported here as viewed from the front and top (top and center rows, respectively) and a Corey-Pauling-Koltun view from the top (ball models in the bottom row). All of the atoms in natural gA are shown in white. The linker atoms are shown in red, and the rest of the chains in the linked dimers are shown in aqua. (**A**) Natural gA; (**B**) gA + (*S*,*S*)-linker, matched pair; (**C**) gA + (*R*,*R*)-linker on the outside, mismatched pair; (**D**) gA + (*R*,*R*)-linker on the inside, mismatched pair.

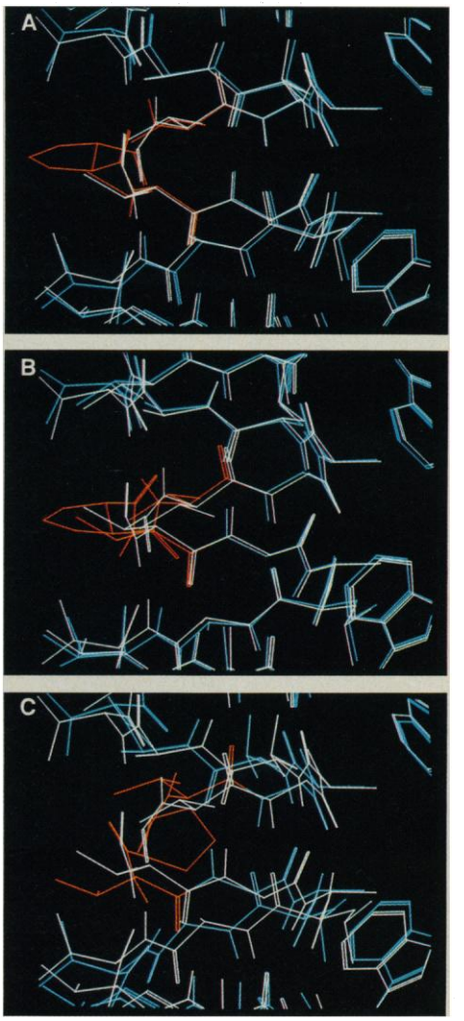

Fig. 3. Superimpositions of the linked dimers with natural gA. All structures are derived from theoretical coordinates for gA. All of the atoms of natural gA are shown in white. Linker and backbone atoms of the first amino acid in each direction from the linker are shown in red. The remaining atoms in the linked dimer are shown in aqua. (**A**) Superimposition of gA and the (*S*,*S*)-linked dimer (matched pair). (**B**) Superimposition of gA and the (*R*,*R*)-linked dimer with the linker on the outside (mismatched pair). (**C**) Superimposition of gA and the (*R*,*R*)-linked dimer with the linker on the inside (mismatched pair).

neighbor peptide backbone atoms was calculated to be 0.58 Å [the (*S*,*S*)-conformer depicted in Figs. 2B and 3A has an rms deviation of 0.20 Å]. The (*R*,*R*)-conformer in Figs. 2D and 3C results in an obvious and significant interference within the channel. Because the orientation of the carbonyl vectors in the right-handed (Ovchinnikov) helix are identical to those in the left-handed (Urry) helix, the chiral linker described in this report cannot differentiate between these two possibilities (compare Fig. 1, B and D).

The synthesis of the tartaric acid–gA hybrids (**1** and **2**) was achieved by a modification of the method reported by Weiss and Koeppe (*15*). Desformyl gA was prepared by the reported method (*1*) from gA that was purified (*16*) from the commercially available mixture of gramicidins. A diphenylphosphoryl azide (DPPA)–mediated coupling reaction provided **1** (from **3**) and **2** (from **4**) in 55% and 60% yields, respectively (*17*). The resultant tartaric acid–gA hybrids were purified by high-performance liquid chromatography (HPLC) and displayed ^{1}H nuclear magnetic resonance (NMR) and fast-atom bombardment mass spectrometry spectra (parent ion peak $M^+ = 3834$) fully consistent with the assigned structures (*18*).

Electrical recordings from lipid bilayers containing **1** or **2** revealed that these molecules form long-lived channels but with significant differences in their conductance properties. The recordings were made from glycerol-monoolein bilayers formed on the tips of borosilicate patch-clamp pipettes as described by Sigworth *et al.* (*19*); typically, 1 μl of 2×10^{-9} *M* gA was added to 5 ml of saline. Currents were measured in symmetrical 640 m*M* KCl solutions with a patch-clamp amplifier and stored in digitized form on video tape.

Both the (*S*,*S*)- and the (*R*,*R*)-linked dimers form long-lived conductance states (Fig. 4, B and C) in which stepwise increases in the conductance indicate the insertion of functional channels into the bilayer. The finite duration (typically 30 min) of a single conductance experiment provides a lower limit estimate of the lifetime of the synthetic "dimeric" channel (*20*). This compares with a channel lifetime for natural gA of several seconds to minutes (Fig. 4A) under identical conditions. The current-voltage (*I-V*) relations of the channels were measured by application of voltage ramps of ±400-mV amplitude (Fig. 5). In addition to the smaller conductance associated with the (*R*,*R*)-dimer, the difference in the shapes of the *I-V* curves for the two dimers is striking. Whereas the *I-V* relation of the (*S*,*S*)-dimer is almost linear in the range explored (similar to that of natural gA), the *I-V* relation of the (*R*,*R*)-dimer is strongly hyperlinear. The computer-generated models of the (*R*,*R*)-linked dimer suggest the existence of a structural distortion at the

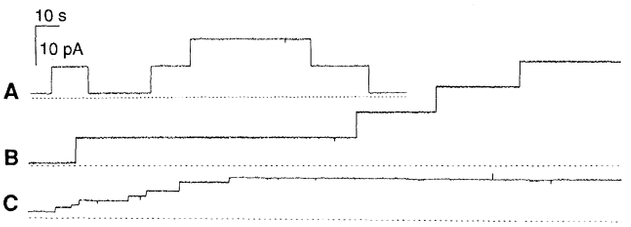

Fig. 4. Single-channel recordings from microbilayers on the tips of patch-clamp pipettes in which stepwise increases in conductance indicate the insertion of functional channels into the bilayer. The artificial membranes were formed from glycerol-monoolein in squalene (40 mg/ml) as described in (*19*). The traces were recorded in symmetrical 640 m*M* KCl solutions at a membrane potential of 200 mV. The effective bandwidth is approximately 50 Hz. In contrast to natural gA (**A**), both the (*S*,*S*)-linked (**B**) and the (*R*,*R*)-linked (**C**) gA dimers form long-lived ion channels (opening in the upward direction). The long lifetimes observed in (B) and (C) are indicative of linked dimers, and the differences in their conductances relative to natural gA can be used as a measure of the matched and mismatched nature of their linkers. Under the described experimental conditions, the average single-channel current through the (*R*,*R*)-dimer for *N* channels is 1.19 (±0.13) pA, $N = 9$, as compared with 6.01 (± 0.10) pA, $N = 40$, for the (*S*,*S*)-dimer, and 6.50 (± 0.04) pA, $N = 39$, for natural gA.

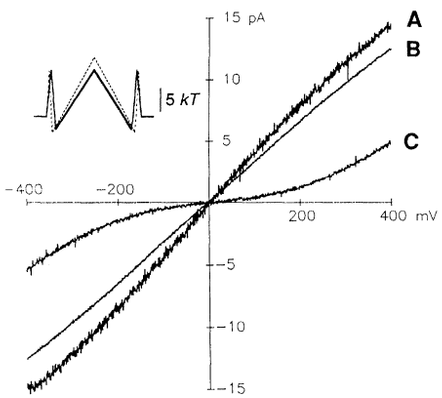

Fig. 5. Currents through (curve A) natural, (curve B) (*S*,*S*)-linked, and (curve C) (*R*,*R*)-linked gA were recorded in response to voltage ramps of ±400-mV amplitude and 10-s duration in symmetrical solutions of 640 m*M* KCl. The (*S*,*S*)-dimer behaves similarly to natural gA, having an *I-V* relation only slightly saturating at high potentials. The *I-V* relation of the (*R*,*R*)-dimer, however, is strongly hyperlinear, suggesting an increase in the height of the central barrier for ion permeation. The inset shows the apparent potential profile of the (*S*,*S*)-dimer (solid line) and the (*R*,*R*)-dimer (dashed line) in units of kT for the passage of a single ion through the channel at zero membrane potential, plotted as a function of the relative electrical distance across the membrane.

amino termini of the peptide chains; accordingly, an increase in the energy barrier for ion transport at the center of the channel was anticipated. In order to further examine this issue, we modeled the permeation process by a two-site, three-barrier scheme as reported by Finkelstein and Andersen (*21*). This model predicts that the current for natural gA is limited mainly by the entry barrier, which represents the diffusion-limited association of ions to the first binding sites. The central barrier is rather shallow and becomes almost negligible at high applied voltages. We applied this model to the two linked dimers by adjusting the conductance parameters (by least-squares methods) to fit the observed *I-V* curves. Although most of the parameters are comparable to those derived for natural gA, the rate of translocation (t_r) over the central barrier had to be decreased by a factor of 32 in order to fit the *I-V* relation of the (*R*,*R*)-dimer (see Table 1). If permeation is simplified to a process that obeys Eyring rate theory, the energy barriers (ΔG) can be obtained from the rate constants according to the equation: rate = $kT/h \exp(-\Delta G/kT)$, where k is Boltzmann's constant, T is the absolute temperature, h is Planck's constant, and ΔG is the Gibbs free energy (*22*). The inset in Fig. 5 illustrates the calculated potential profiles for the passage of one ion through the (*S*,*S*)- and (*R*,*R*)-linked dimers.

These findings correlate well with the computer simulations (Figs. 2 and 3), which predicted that the (*S*,*S*)-linked dimer would result in a matched head-to-head junction, whereas the (*R*,*R*)-linkage would cause local distortions in the linking region and thus increase the energetic barrier to ion transport. One additional finding may be relevant to this structural analysis. For the (*R*,*R*)-isomer, brief closures to zero conductance (flickers) are observed during the long single-channel events; at 20°C, these flickers have an average lifetime of about 100 μs and occur at a rate of 100 per second. The (*S*,*S*)-linked dimer shows no such flickers (*23*). Modeling studies suggest that the conformer with the dioxolane ring of the (*R*,*R*)-linker inside the ion channel is comparable in energy to the conformer with this element outside the channel. An equilibrium between these two isomers may therefore be responsible for the flickering observed in the conductance for the (*R*,*R*)-linked dimer. Further experimentation will be required to understand the precise molecular mechanism of this phenomenon and to control the gating of these hybrid ion channels.

REFERENCES AND NOTES

1. R. Sarges and B. Witkop, *J. Am. Chem. Soc.* **87**, 2011 (1965); *ibid.*, p. 2020; *ibid.*, p. 2027; *Biochemistry* **4**, 2491 (1965).
2. For two recent reviews, see: B. Cornell, *J. Bioenerg. Biomembr.* **19**, 655 (1987); O. S. Andersen, *Annu. Rev. Physiol.* **46**, 531 (1984).
3. M. Veatch and L. Stryer, *J. Mol. Biol.* **113**, 89 (1977).
4. D. A. Langs, *Science* **241**, 188 (1988).
5. B. A. Wallace, *Biophys. J.* **49**, 295 (1986); _____ and K. Ravikumar, *Science* **241**, 182 (1988).
6. S. Weinstein, B. A. Wallace, E. R. Blout, J. S. Morrow, W. Veatch, *Proc. Natl. Acad. Sci. U.S.A.* **76**, 4230 (1979); S. Weinstein, B. A. Wallace, J. S. Morrow, W. R. Veatch, *J. Mol. Biol.* **143**, 1 (1980); E. Bamberg, H. J. Apell, H. Alpes, *Proc. Natl. Acad. Sci. U.S.A.* **74**, 2402 (1977); H. J. Apell, E. Bamberg, H. Alpes, P. Läuger, *J. Membr. Biol.* **31**, 171 (1977). G. Stark, M. Strässle, and Z. Takacz [*J. Membr. Biol.* **89**, 23 (1986)] have recently proposed that the active channel structure is a dimer of dimers (head-to-head); this hypothesis is based on temperature and voltage jump experiments with gA and malonyl-gA dimer.
7. D. W. Urry, M. C. Goodall, J. D. Glickson, D. F. Mayers, *Proc. Natl. Acad. Sci. U.S.A.* **68**, 1907 (1971).
8. D. W. Urry, J. T. Walker, T. L. Trapane, *J. Membr. Biol.* **69**, 225 (1982); D. W. Urry, T. L. Trapane, K. U. Prasad, *Science* **221**, 1064 (1983).
9. A. S. Arseniev, I. L. Barsukov, V. F. Bystrov, A. L. Lomize, Y. A. Ovchinnikov, *FEBS Lett.* **186**, 168 (1985).
10. J. D. Lear, Z. R. Wasserman, W. F. DeGrado, *Science* **240**, 1177 (1988); V. E. Carmicheal *et al.*, *J. Am. Chem. Soc.* **111**, 767 (1989); L. Jullien and J.-M. Lehn, *Tetrahedron Lett.* **29**, 3803 (1988), and references therein.
11. The left-handed helix has been reported: B. Roux and M. Karplus, *Biophys. J.* **53**, 297 (1988). The right-handed helix was constructed with the dihedrals reported by Ovchinnikov; see (*9*).
12. These are helical structures analogous to β sheets (but rolled into helices) in which the repeating unit is a dipeptide. β Helices are found in peptide sequences that contain alternating D- and L-amino acids: see R. E. Koeppe II and M. Kimura, *Biopolymers* **23**, 23 (1984).
13. We prepared the bis-acids **3** and **4** by heating the corresponding diethyl tartrate in diethoxy methane, using a catalytic amount of *p*-toluenesulfonic acid (pTsOH), which resulted in the formation of the intermediate bis-ethoxymethyl ether. Slow distillation of the excess diethoxymethane resulted in the loss of one equivalent of diethoxymethane and formation of the desired dioxolane (Me, methyl; Et, ethy; Ph, phenyl). This crude product was then purified by flash chromatography on silica gel [W. C. Still, M. Kahn, A. Mitra, *J. Org. Chem.* **49**, 576 (1978)]. Subsequent saponification, acidification, extraction, and recrystallization (from ethyl acetate) yielded the desired bis-acids. ^{1}H NMR in CH_3OH-d_4: δ 5.2 (s, 2H, OCH_2O), 4.75 (s, 2H, CH) relative to CH_3OH-d_3(H). **3** (*S*,*S*): $[\alpha]_D^{25} = +77.0°$ (specific rotation relative to the sodium D line at 25°C) (c 0.985, H_2O). **4** (*R*,*R*): $[\alpha]_D^{25} = -77.7°$ (c 1.01, H_2O) (s, singlet; c, concentration in grams per 100 ml).
14. Structures were generated with the MACROMODEL V2.0 molecular modeling software package (W. C. Still, Columbia University) and were minimized with the OPLS-A force field with an electrostatic cutoff of 8 Å [see W. L. Jorgensen and S. Tirado-Rives, *J. Am. Chem. Soc.* **110**, 1657 (1988)]. Minimizations were run until the first-derivative (rms gradient was <0.01 kJ/Å with the use of the Polak-Ribiere conjugate gradient algorithm [E. Polak and G. Ribiere, *Rev. Fr. Inf. Rech. Oper.* **35**, 16 (1969)]. For the superimpositions, the deviations are based on rigid superimposition of the backbone atoms of the linker and the first amino acid in each direction, including the carbonyl oxygen and the amide hydrogen.
15. L. B. Weiss and R. E. Koeppe II, *Int. J. Pept. Protein Res.* **26**, 305 (1985), and references therein.

16. C. J. Stankovic, J. M. Delfino, S. L. Schreiber, in preparation.
17. The linked dimers **1** and **2** were prepared as follows. We prepared gA from the commercially available mixture (gA′) by flash chromatography on silica gel, using chloroform:methanol:water:acetic acid (~400:30:4:1) [for further details see (*16*)]. gA was then deformylated (*1*) with anhydrous hydrogen chloride in methanol (generated from acetyl chloride and methanol). Desformyl gA was purified on AG-MP-50 and Sephadex LH-20. The coupling was accomplished according to the method of Weiss and Koeppe (*15*). DPPA was added to a solution of the bis-acid and desformyl gA in *N*,*N*-dimethylformamide (DMF) at −20°C, and then triethylamine was added. The resulting solution was kept at 0°C for 24 to 48 hours, then warmed to room temperature and quenched with methanol. The DMF was then removed by vacuum evaporation. Purification of the crude product by Sephadex LH-20, ion-exchange chromatography with AG-MP 50, silica gel chromatography, and ion-exchange chromatography with AG-501 yielded the desired dimers. A sample of these products was further purified by reversed-phase HPLC on a Beckman C-18 column (10 by 250 mm) with methanol:water (95:5) at 3 ml/min to provide a highly purified sample for conductance studies.
18. The ^{1}H NMR spectra of both dimers are nearly identical to that of gA (*7*) except for the appearance of two new singlets, associated with the linker, with the expected integrations. Spectra were recorded on a Bruker 500-MHz ^{1}H NMR in DMSO-d_6 with δ values reported relative to DMSO-d_5(H) (DMSO, dimethyl sulfoxide). (*S*,*S*)-linked dimer **1**: δ 5.15 (s, 2H, OCH_2O), 4.65 (s, 2H, CH). (*R*,*R*)-linked dimer **2**: δ 5.1 (s, 2H, OCH_2O), 4.55 (s, 2H, CH). In each case the signal for the hydroxyl proton for the ethanolamine is still present and integrates correctly for two protons, indicating that these dimers are linked amino terminus to amino terminus. The R_f values in chloroform:methanol:water:acetic acid (100:30:4:1) are as follows: gA (0.71), desformyl gA (0.37), (*S*,*S*)-linked dimer **1** (0.20), and (*R*,*R*)-linked dimer **2** (0.66). S. Weinstein, J. T. Durkin, W. R. Veatch, and E. R. Blout [*Biochemistry* **24**, 5249 (1984)] have used the ratio of the absorbance at 320 nm to that at 290 nm as an indication of the absence of degradation of the tryptophans in gA. For the linked dimers, the corresponding ratios [(*S*,*S*)-linked dimer **1** (0.033) and (*R*,*R*)-linked dimer **2** (0.061)] indicate that little if any appreciable degradation has occurred. We have observed that this degradation can also be estimated by analysis of the aromatic region of the ^{1}H NMR spectra, which shows new signals for the degradation product.
19. F. J. Sigworth, D. W. Urry, K. U. Prasad, *Biophys. J.* **52**, 1055 (1987).
20. Another possible limitation is the finite functional lifetime of a channel diffusing within a bilayer with a radius of only ~5 μm.
21. A. Finkelstein and O. S. Andersen, *J. Membr. Biol.* **59**, 155 (1981).
22. Ions must travel a considerable distance between two binding sites; accordingly, this description is rather simple and serves only as a qualitative description of the physical system. For a review of the problem of transforming transition rates into energy profiles, see K. E. Cooper, P. Y. Gates, R. S. Eisenberg, *Q. Rev. Biophys.* **21**, 331 (1988).
23. S. H. Heinemann *et al.*, *Biophys. J.* **55**, 505a (1989).
24. S.L.S. was supported by the National Institute of General Medical Sciences; C.J.S. was the recipient of a graduate fellowship from Pfizer, Inc.; J.M.D. was supported by the John E. Fogarty International Center and the CONICET (Consejo Nacional de Investigaciones Científicas y Técnicas) Republica Argentina; F.J.S. was supported under NIH grant NS-21501; S.H.H. was supported in part by the German Academic Exchange Service. We thank M. Karplus and B. Roux for providing the coordinates for the left- and right-handed gA helix dimers and G. Glick and B. Roux for helpful suggestions regarding molecular modeling.

23 December 1988; accepted 3 March 1989

Class II MHC Molecules Are Specific Receptors for Staphylococcus Enterotoxin A

JOSEPH A. MOLLICK, RICHARD G. COOK, ROBERT R. RICH

T cell proliferation in response to stimulation with *Staphylococcus* enterotoxin A (SEA) requires accessory cells that express class II major histocompatibility complex (MHC) molecules. Murine fibroblasts transfected with genes encoding the α and β subunits of HLA-DR, DQ, or DP were used to show that the proliferative response of purified human T cells to SEA is dependent on class II molecules but is not restricted by the haplotype of the responder. Binding of fluoresceinated SEA to class II transfectants and precipitation of class II heterodimers with SEA-Sepharose show that the proliferative response is a result of SEA binding to class II molecules. The binding is specific for class II molecules and is independent of class II allotype or isotype. The ability of SEA to bind class II molecules may be a general characteristic of this class of antigens, now called "superantigens."

STAPHYLOCOCCAL ENTEROTOXINS ARE a family of molecules, encoded by bacteriophages, that cause staphylococcal food poisoning (*1*). These proteins are also powerful T cell mitogens; like other mitogens they cause T cell activation and proliferation in the presence of accessory cells (*2*). However, unlike most mitogens, SEA also requires cells with MHC class II molecules on their surface for presentation to T cells (*3, 4*). Because protein antigens, but not mitogens, are dependent on interactions with MHC class II molecules for presentation to and activation of $CD4^+$ T cells, we investigated the role of class II molecules in the T cell reponse to SEA.

Because class II antigen expression is characteristic of most conventional antigen-presenting cells, we used mouse fibroblasts transfected with both HLA class II α and β chains to assess the role of these molecules independent of the accessory cell signals supplied by the fibroblasts. Purified T cells from one individual were tested with a panel of transfected fibroblasts that includes members of the three isotypes of HLA class II antigens (DR, DQ, and DP) (Fig. 1). Each of the transfected fibroblasts supported proliferative responses to SEA, regardless of the allotype or class II isotype of the transfected gene. Untransfected cells and HLA class I–transfected fibroblasts did not support proliferative responses at any SEA concentration. All of the fibroblast lines similarly supported a phytohemagglutinin response, whether or not class II molecules were present.

These data, along with reports that SEA does not require cellular processing to stimulate T cells (*3*), were indicative of the possibility that SEA binds directly to class II molecules to form a complex that interacts with T cell receptors in a largely MHC-unrestricted fashion. We therefore used flow cytometry to assess the binding of fluoresceinated SEA (Fig. 2). SEA could bind to the human B cell line Raji but not to RJ2.2.5, a class II–negative mutant of this line that expresses class I molecules but does not express any of the three class II isotypes (*5*). Similarly, SEA could bind to HLA-DR1–transfected fibroblasts but not to the untransfected parental cells. Specific binding to resting T cells was not observed. The capacity to bind class II antigens was also tested by immunoprecipitation with SEA from detergent lysates of cells surface-labeled with ^{125}I. SEA bound two proteins from the B cell line Raji that migrated with DR α and β polypeptides that could be precipitated with L243, a monoclonal antibody to the class II DR isotype (Fig. 3) (*6*). Neither SEA nor L243 precipitated these proteins from the class II–negative mutant RJ2.2.5. Similarly, SEA bound the class II heterodimer from mouse fibroblast lines transfected with either of two different DR alleles, or with DQ or DP (*7*). We investigated the possibility that SEA also bound a ligand on the responding cells—for example, the T cell receptor. However, SEA did not bind any iodinated cell surface proteins from purified T cell lysates (Fig. 3), indicating that native SEA does not bind the T cell receptor or other cell surface molecules with a high-affinity interaction similar to that involved in binding class II molecules. This does not rule out the possibility that SEA may bind directly to T cell receptors with a substantially lower affinity or to a subset of

Howard Hughes Medical Institute Laboratory and Department of Microbiology and Immunology, Baylor College of Medicine, Houston, TX 77030.